Appl. Phys. A 83, 271–275 (2006)
DOI: 10.1007/s00339-006-3490-7

Applied Physics A
Materials Science & Processing

L. LANDSTRÖM
N. ARNOLD
D. BRODOCEANU*
K. PIGLMAYER
D. BÄUERLE✉

Photonic properties of silicon-coated monolayers of colloidal silica microspheres

Institut für Angewandte Physik, Johannes-Kepler-Universität Linz, 4040 Linz, Austria

Received: 8 December 2005/Accepted: 13 December 2005
Published online: 31 January 2006 • © Springer-Verlag 2006

ABSTRACT The spectral dependence of the optical transmission through close-packed monolayers of silica (a-SiO_2) microspheres covered with different amounts of amorphous silicon (a-Si) is studied. The strong dips in the transmission can be understood by the coupling of the incident electromagnetic field into the modes of the combined photonic slab structure consisting of the close-packed lattice of a-SiO_2 microspheres and a-Si. The dependence of the transmission minima positions on the a-Si thickness and the angle of incidence agree quite well with model calculations.

PACS 78.66.-w; 81.16.Dn; 82.70.Dd; 42.70.Qs

1 Introduction

Regular two-dimensional (2D) periodic lattices of microspheres can be formed over relatively large areas in a self-assembling process from colloidal solutions. Such monolayers (ML) can be employed as microlens arrays for single-step parallel laser processing [1–5]. There exist, however, a number of other interesting applications. Regular lattices of microspheres with diameter d having lattice constants of the order of λ show Bragg resonances and photonic band effects, which permit to manipulate electromagnetic waves at optical frequencies (photonic crystals). Subsequently, we concentrate on 2D lattices of dielectric microspheres, which represent photonic crystal slabs (PCS) [6]. The optical properties of such bare lattices have been studied in [7, 8]. To expand the functionality of this easily produced system and customize it for the desired wavelengths and applications, we recently demonstrated that the optical properties of such monolayers can be significantly altered by metal coatings [9]. Such structures demonstrate phenomena similar to extraordinary transmission through sub-wavelength apertures [10, 11]

In the present paper we report on ML of dielectric microspheres that are covered with different amounts of amorphous silicon (a-Si). The photonic properties of such "mixed" structures can be tuned not only via the size of spheres, but also via the thickness of the deposited layer. Both of them modify the effective refractive index and change the structure of the propagating eigenmodes.

2 Experiment

The ML lattices of microspheres were formed from a colloidal solution on a quartz support and coated with different a-Si film thicknesses using standard e-beam evaporation. As with metal-coated ML discussed in [9], only the upper half of each sphere is silicon-coated. The thickness of the coating at the top of spheres is about equal to that measured by a nearby quartz-crystal microbalance (QCM). In the interstices between the spheres, the coating is deposited onto the quartz support.

3 Results and discussion

The optical transmission spectra shown in Fig. 1 for both coated and uncoated ML were recorded at normal incidence by means of a UV- to near-IR-spectrometer (Cary 500) with non-polarized light. The most pronounced features in the optical spectrum for uncoated ML (upper curve) are the overall decrease in transmitted intensity towards shorter wavelengths and the dip at $\lambda \approx 1585$ nm. There are also indications for other features at shorter wavelengths. For stochastic lattices fabricated by pulsed-laser deposition (PLD) [12] from a pellet of microspheres, the dip at 1585 nm vanishes. Thus, this feature is definitely related to the translational symmetry of the 2D lattice. If we cover the ML with a layer of a-Si, the main dip at 1585 nm and the features at shorter wavelengths become more pronounced and simultaneously shift. This effect increases with the thickness of the a-Si layer which was varied between 25 nm and 300 nm.

These observations can be explained as follows. The overall decrease in zero order transmission with decreasing wavelength is due to destructive interference of virtual sources from a single primitive cell of the hexagonal lattice.

✉ Fax: ++43 2468-9242, E-mail: dieter.baeuerle@jku.at
*Also at NILPRP Bucharest

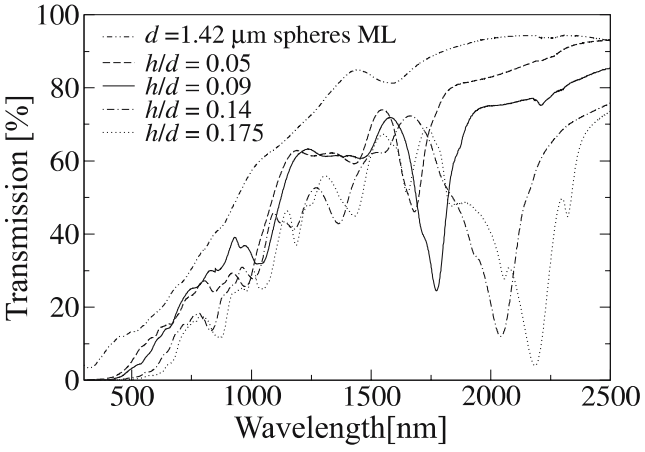

FIGURE 1 Transmission spectra measured at normal incidence for monolayers (ML) of a-SiO_2 microspheres ($d = 1.42\,\mu$m) covered with a-Si layers of different thicknesses. The *upper curve* refers to an uncoated lattice

This decrease may be further enhanced by parasite scattered radiation that is not collected by the spectrometer. The dip in transmitted intensity that appears at 1585 nm, which deepens and redshifts with the thickness of deposited silicon, is related to first order diffracted waves. The ML of silica spheres with the deposited a-Si layer is a 2D PCS, which can support propagating Bloch modes. If one or several higher order diffracted waves propagate at a grazing angle to the plane of translational symmetry of the monolayer (which we denote as x–z), they may efficiently couple to the photonic modes supported by such a composite slab. Due to overall energy conservation, this coupling will cause an attenuation of the zero-order transmitted intensity. In the theory of diffraction gratings, this is known as the Rayleigh–Wood anomaly [13].

The deposition of a-Si onto a-SiO_2 ML results in a much higher refractive index contrast as interstices are filled. The structure starts to resemble a 2D inverted artificial opal, which in 3D exhibits true band gaps and other nontrivial optical properties [14]. Thus, an increase in thickness of sputtered a-Si results in a more pronounced structure of the photonic modes revealed in the shift of the transmission dips and their intensification (see Fig. 1).

Quantitative comparison with the experimentally determined transmission is difficult for several reasons. The light used in the spectrometer is nonpolarized. The monolayer of spheres is not perfect over large areas, but consists of ordered domains of about hundred μm in size. Even for a single domain, when only first order diffraction is considered, light may couple into several (degenerate) modes simultaneously, with different efficiencies, depending on polarization. Thus, the measured transmission results from complex averaging over orientation of polarization with respect to reciprocal lattice vectors, which is difficult to control experimentally. Finally, the exact geometry and optical parameters of the a-Si deposit depend on the sputtering conditions. The refractive index of a-Si may vary within the range $3 < n(\text{a-Si}) < 5$ for $0.3\,\mu\text{m} < \lambda < 2.5\,\mu\text{m}$ [15]. For these reasons we concentrate on the overall dependence of dip positions on various parameters and use well-defined polarization and constant optical properties in the calculations.

The positions of dips in transmission can be estimated in the following way: The wavevector $\boldsymbol{k}'$ of diffracted waves satisfy the Bragg condition $\boldsymbol{k}' = \boldsymbol{k} + \boldsymbol{G}$, where $\boldsymbol{k}$ is the wavevector of incident light and $\boldsymbol{G}$ an arbitrary reciprocal lattice vector. Efficient coupling may occur if the in-plane component of the diffracted wave will coincide with the wavevector $\boldsymbol{k}_s(\omega)$ of some of the modes propagating along the slab for light frequency ω. Analysis of such modes requires consideration of full 3D vectorial Maxwell equations as these modes are usually confined to the slab, i.e., are evanescent in the normal (y) direction. Numerical calculations of this kind were performed in [7] for uncoated polystyrene (PS) spheres with a refraction index of $n(\text{PS}) = 1.6$. They give reasonable agreement with our measured spectra for monolayers of PS spheres without the deposit.

Our goal in this letter is, however, to study the behavior of monolayers of silica spheres covered with different amounts of a-Si. Here, the general condition for the coupling can be written as

$$\begin{aligned}\boldsymbol{k}_s(\omega) &= \boldsymbol{k}_\parallel + \boldsymbol{G} \\ &= \boldsymbol{k}\sin\theta + m_1\boldsymbol{b_1} + m_2\boldsymbol{b_2}\,, \end{aligned} \qquad (1)$$

where $\boldsymbol{b_{1,2}}$ are primitive vectors of the reciprocal lattice, $m_{1,2}$ are integers and θ the angle of incidence. For a 2D hex-

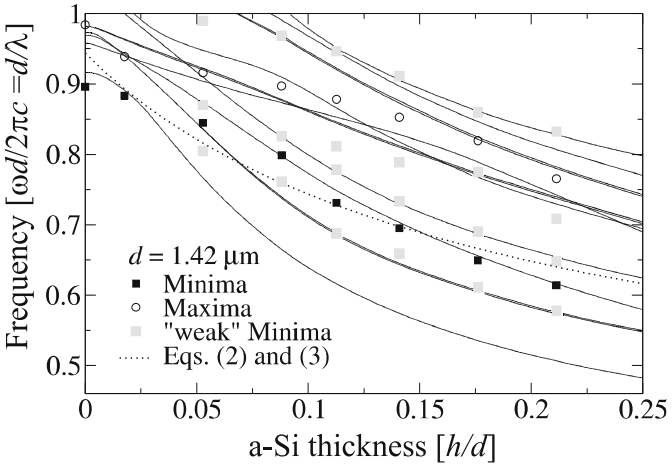

FIGURE 2 Frequencies of the lowest modes at Γ-point as functions of a-Si deposit thickness h. Only confined (not folded) modes are shown. *Dotted curve* – estimation from (2) (at normal incidence $\theta = 0$) and (3). Experimental points are deduced from the dips (*solid squares*) and maxima (*open circles*) in the transmission curves for the microspheres with $d = 1.42\,\mu$m. $n_{SiO_2} = 1.35$ and 1.42 were taken for the spheres and support, respectively, $n_{Si} = 3.3$ for the a-Si layer of thickness h was used

agonal monolayer, the reciprocal lattice vectors are at an angle $\pi/6$ to the lines connecting the centers of adjacent spheres and have the absolute values $b_{1,2} = 4\pi/\sqrt{3}d$.

Let us first consider normal incidence. In this case $\theta = 0$, and one obtains from condition (1) that in the reduced zone scheme the relevant wavevectors $\boldsymbol{k}_s(\omega)$ correspond to the center of the first Brillouin zone (Γ-point). Therefore, the dips at normal incidence correspond to the lowest modes at Γ-point. Figure 2 shows the calculated dependence of the (normalized) frequency of such modes on the thickness of the deposited silicon. The structure included the monolayer of spheres and the deposit. The deposit on top of the spheres was modeled as an additional a-Si sphere, with lower refractive index priority, shifted up by the thickness of the deposit h. The deposit in the interstices was modeled as a film of the same thickness, perforated by the hexagonal array of cylinders of diameter d with the axes passing through the spheres' centers normal to the support. The calculations were performed using a $2d$ supercell in y-direction, which necessitated mode selection. The relevant modes that do not originate from the folding in y-direction were found by visual inspection of the mode profiles. Two of them are shown in Fig. 3. Because such modes are strongly confined to the monolayer and (due to high refractive index of the deposit) in particular to the a-Si film, they are more sensitive to the changes in the thickness h. For the same reason (unlike in [8]), they are also rather insensitive to the presence and thickness of the support (which was not included into calculations in Fig. 2 as it led to many spurious modes). Finally, with increasing supercell size the physical modes remain almost the same, while the number and the energy of folded modes changes strongly.

Not all slab modes contribute equally to transmission changes. The coupling process is illustrated in Fig. 4, which gives examples of FDTD (finite difference time domain) calculations for different parameters of the composite structure. In Fig. 4a the resonant excitation propagates along the layer far beyond the incident Gaussian beam. The value $\lambda = 1.54d$ used in this case corresponds to the main dip in transmission for this thickness of the deposit (see Figs. 1 and 2). The mode (tentatively) responsible for the main dip is shown in Fig. 3b. Because of the sixfold symmetry of the depicted mode, efficient coupling may occur into six directions simultaneously for both polarizations. For the case $\lambda = 1.22d$, Fig. 4b, which corresponds to a transmission peak (see Figs. 1 and 2), the coupling is almost absent. Interestingly, poor coupling (similar to that seen in Fig. 4b) was also observed for the lowest, "donut" mode (see Figs. 2 and 3a), which for $h = 0$ originates from the lowest Mie mode. Light coupling into this mode is weak, as it has the azimuthal structure of the electric field similar to that

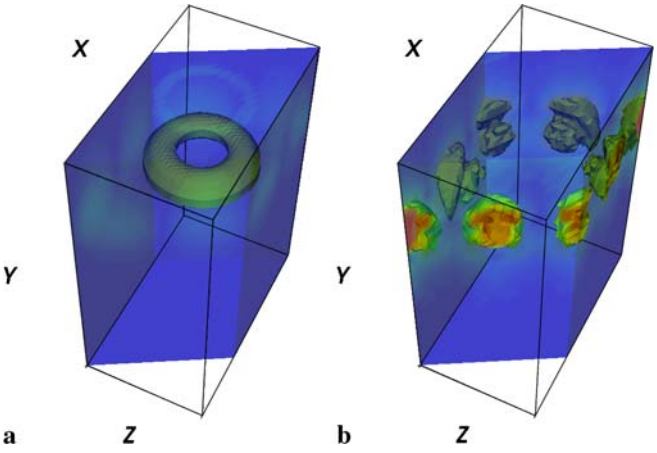

FIGURE 3 Distribution of intensity $\boldsymbol{EE}^*$ in two of the modes at the Γ-point. Deposit thickness $h = 0.175d$. (**a**) Donut mode; (**b**) The mode tentatively responsible for the most pronounced dip in transmission. Other parameters are as in Fig. 4

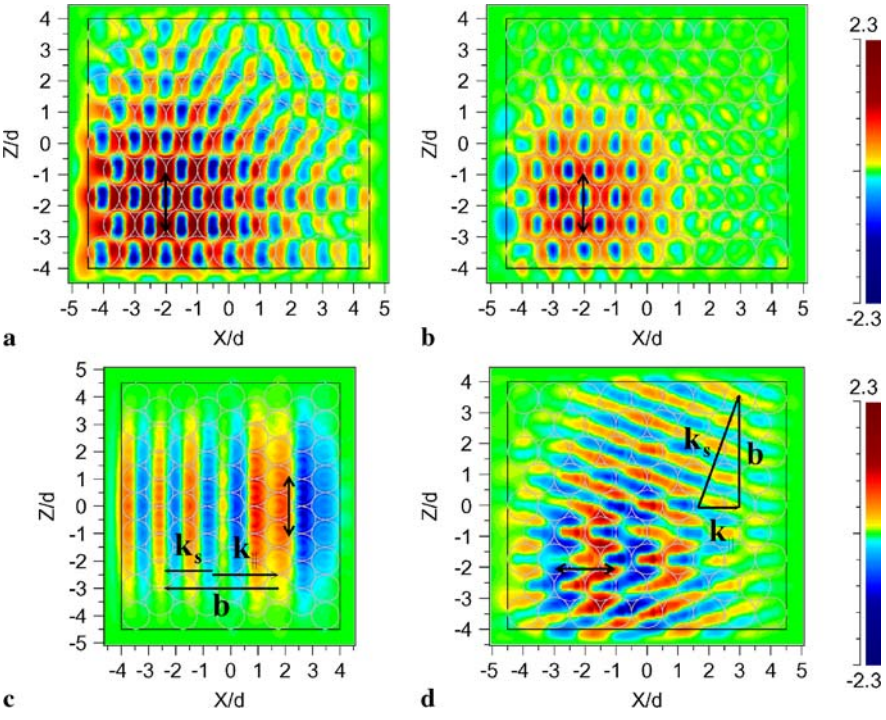

FIGURE 4 FDTD calculations of the light coupling into composite monolayer. Material parameters as in Fig. 2. Field component corresponding to the polarization of incident Gaussian beam (↕ or ↔) is shown at $y = 0.5d$ (*top of the spheres*). Beam with half-width (1/e field) $w_0 = 2.5d$ centered at $x = -2d$, $z = -2d$ and at $x = -2d$, $z = 0$ for (**c**). (**a**) Normal incidence, $h/d = 0.175$ and $\lambda/d = 1.54$. This corresponds to the main measured dip seen in Fig. 1. Its h dependence is shown in Fig. 2 and the responsible mode in Fig. 3b. (**b**) Same as (**a**) but for $\lambda/d = 1.22$, corresponding to transmission maximum seen in Figs. 1 and 2. (**c**) Oblique incidence ($\theta = \pi/6$ in x–y plane). $h/d = 0.11$ and $\lambda/d = 1.6$. Diffraction on $\boldsymbol{b}$ vector with $\varphi = \pi$ is responsible for the *lowest dashed curve* in the *inset* in Fig. 5. (**d**) Same as (**c**) but $\lambda/d = 1.23$. Strong diffraction on $2\,\boldsymbol{b}$ vectors with $\varphi = \pm\pi/2$ is responsible for the *upper curve* in Fig. 5 (*inset*)

described in [16] in each sphere. In general, it is difficult to resolve various modes experimentally, because of the aforementioned inaccuracies in orientation, polarization, shape of deposit and material parameters. The agreement in Fig. 2 can be improved using these factors, but this amounts to little more than curve fitting.

Let us now discuss the angular dependence of the zero order transmission. Experimental results are presented in Fig. 5. Considering the resonant condition (1) in the first Brillouin zone, we arrive at $\boldsymbol{k}_s(\omega) = \boldsymbol{k}\sin\theta$. Therefore, the dependence of the dip positions on the in-plane component of the incident wavevector, determined by the wavelength, angle of incidence and orientation of the incident light, should reproduce the ω contour of the frequency surface. However, the true eigenvalues of a PCS responsible for the transmission changes are complex [7], and cannot be easily studied in supercell formalism at oblique incidence. In addition, domain structure of the monolayer does not allow direct comparison for the given polarization and well defined direction (e.g., to M or K points in the Brillouin zone). For these reasons we adopt a simple approach that nevertheless captures the essence of the measured angular dependence.

As we pointed out in [17], some of the observed features can be understood semi-quantitatively using the concept of effective refractive index. Let us assume that the coupling into some mode with the effective refractive index n_{eff} takes place via reciprocal lattice vector $\boldsymbol{G}$ at an angle φ with the plane of incidence. Then, square of the vector resonant condition (1) results in the expression $n_{\text{eff}}^2 k^2 = k^2\sin^2\theta + G^2 + 2Gk\sin\theta\cos\varphi$, which can be resolved for λ. For example, assuming first order diffraction, i.e., $G = b = 4\pi/\sqrt{3}d$ we obtain:

$$\lambda = \frac{d\sqrt{3}}{2} \times \left(\sqrt{n_{\text{eff}}^2 - \sin^2\theta\sin^2\varphi} - \sin\theta\cos\varphi\right). \quad (2)$$

For first order diffraction there always exist six vectors to couple to with the angle $\pi/3$ between them. As the monolayer is not perfectly ordered, the observed dips are the result of averaging over the angle φ. This averaging is weighted with the coupling efficiencies, which also depend on polarization. FDTD results indicate (Fig. 4c), that for oblique incidence at not too small θ angles, the main dip has better coupling for s-polarization if $\boldsymbol{b}$ vectors are at $\varphi = \pi$ and $\varphi = 5\pi/6$ (not shown). Note, that in the latter case, there exist two modes and that both polarizations may couple into both of them, thus increasing the overall efficiency. At small θ angles, all φ angles almost equally contribute to coupling, which results in a flattening of the corresponding dispersion curve (see inset Fig. 5). The p-polarization couples preferentially into the reciprocal lattice with $\varphi = \pi/2$, see Fig. 4d. For s-polarization, E_x component of the field still appears from scattering, and light couples into the same modes as in Fig. 4d, albeit somewhat weaker. Thus, there is a preferential coupling to modes with wavevector perpendicular to the polarization direction. This effect can be qualitatively explained by the fact that individual elementary dipoles of the slab material (mainly Si) do not scatter along the dipole axis (i.e., in the direction of polarization). The dispersion curves for these φ angles are shown in the inset in Fig. 5 by dashed lines. Modes responsible for this splitting of the main dip are related. Both are sixfold degenerate, but rotated with respect to each other by $\pi/6$. The mode with lower energy (depicted in Fig. 3b) is localized in the sphere contact region, while the other in the deposit near the interstices. This, most likely, explains their difference in energy at normal incidence. We took the value of n_{eff} from the fit to experimental values at normal incidence. But, for the main dip, one can also estimate n_{eff} on the basis of filling factors, and get a qualitative picture of the dependence of transmission dips on material parameters and structure geometry. Filling factor for a single uncoated hexagonal ML $f = \pi/3\sqrt{3} \approx 0.6$ was used in [17]. We extend this expression to a more general law described by the power parameter p: $n_{\text{mon}}^p = n_{\text{SiO}_2}^p f + 1^p(1-f)$. For example $p = 2$ corresponds to a volume average of dielectric functions, $p = 2/3$ to the so-called LLL rule, etc. Finally, we take into account the silicon film:

$$n_{\text{eff}}^p = \frac{n_{\text{mon}}^p + n_{\text{Si}}^p h/d}{1 + h/d}. \quad (3)$$

This expression gives a reasonable guideline for the main dip position with $p = 2$ (Fig. 2, dotted curve).

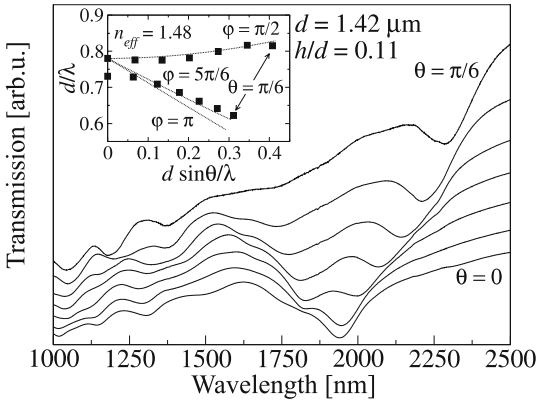

FIGURE 5 Changes in zero-order transmission with the angle of incidence θ. a-Si deposit thickness $h = 0.11d$ with $d = 1.42\,\mu\text{m}$. The *points* in the *inset* (*squares*) are deduced from the transmission dip positions in the main plot. Transmission curves are shifted in y-scale for convenience

4 Conclusions

We conclude that composite slabs consisting of regular lattices of self-assembled colloidal microspheres covered with other materials permit simple fabrication of non-trivial 2D photonic structures. Their optical properties can easily be varied, via the diameter of the spheres and via the thickness of the deposit. The latter dependence is investigated for the first time. There is a good agreement between the experimental and theoretical results.

ACKNOWLEDGEMENTS We thank the Austrian Research Fund FWF (Fonds zur Förderung der wissenschaftlichen Forschung) under contract no. P16133-N08 for financial support. We would also like to thank the "Knut and Alice Wallenberg Foundation" for a postdoctoral

fellowship (L. L.) and the CD Laboratory of Surface Optics, Johannes-Kepler-Universität Linz, for financial support (N. A.).

REFERENCES

1 K. Piglmayer, R. Denk, D. Bäuerle, Appl. Phys. Lett. **80**, 4693 (2002)
2 G. Wysocki, R. Denk, K. Piglmayer, N. Arnold, D. Bäuerle, Appl. Phys. Lett. **82**, 692 (2003)
3 L. Landström, J. Klimstein, G. Schrems, K. Piglmayer, D. Bäuerle, Appl. Phys. A **78**, 537 (2004)
4 B.S. Luk'yanchuk (Ed.), *Laser Cleaning* (World Scientific, Singapore 2002)
5 D.M. Kane (Ed.), *Laser Cleaning II* (World Scientific, Singapore 2005)
6 S. Johnson, S. Fan, R. Villeneuve, J.D. Joannopoulos, Phys. Rev. B **60**, 5751 (1999)
7 H. Miyazaki, K. Ohtaka, Phys. Rev. B **58**, 6920 (1998)
8 Y. Kurokawa, H. Miyazaki, Y. Jimba, Phys. Rev. B **69**, 155 117 (2004)
9 L. Landström, D. Brodoceanu, K. Piglmayer, G. Langer, D. Bäuerle, Appl. Phys. A **81**, 15 (2005)
10 T.W. Ebbesen, H.J. Lezec, H.F. Ghaemi, T. Thio, P.A. Wolff, Nature **391**, 667 (1998)
11 L. Martín-Moreno, F. J. García-Vidal, H.J. Lezec, K.M. Pellerin, T. Thio, J.B. Pendry, T.W. Ebbesen, Phys. Rev. Lett. **86**, 1114 (2001)
12 D. Bäuerle, *Laser Processing and Chemistry* (Springer, Berlin 2000)
13 E.W. Palmer, M.C. Hutley, A. Franks, J.F. Verrill, B. Gale, Rep. Prog. Phys. **38**, 975 (1975)
14 Y.A. Vlasov, X.Z. Bo, J.C. Sturm, D.N. Norris, Nature **414**, 289 (2001)
15 www.ioffe.ru/SVA/NSM/nk/Silicon/Gif/siam1.gif, www.ioffe.ru/SVA/NSM/nk/Silicon/Gif/siam2.gif
16 R. Dorn, S. Quabis, G. Leuchs, Phys. Rev. Lett. **91**, 233 901 (2003)
17 L. Landström, D. Brodoceanu, N. Arnold, K. Piglmayer, D. Bäuerle, Appl. Phys. A **81**, 911 (2005)